

Effects of Tarsal Morphology on Load Feedback During Stepping of a Robotic Stick Insect (Carausius Morosus) Limb

Clarus A. Goldsmith^{1(B)}, William P. Zyhowski¹, Ansgar Büschges², Sasha N. Zill³, Gesa F. Dinges¹, and Nicholas S. Szczecinski¹

Abstract. Sensory feedback from sense organs during animal locomotion can be heavily influenced by an organism's mechanical structure. In insects, the interplay between sensing and mechanics can be demonstrated in the campaniform sensilla (CS) strain sensors located across the exoskeleton. Leg CS are highly sensitive to the loading state of the limb. In walking, loading is primarily influenced by ground reaction forces (GRF) mediated by the foot, or tarsus. The complex morphology of the tarsus provides compliance, passive and active substrate grip, and an increased moment arm for the GRF, all of which impact leg loading and the resulting CS discharge. To increase the biomimicry of robots we use to study strain feedback during insect walking, we have developed a series of tarsi for our robotic model of a Carausius morosus middle leg. We seek the simplest design that mimics tarsus functionality. Tarsi were designed with varying degrees of compliance, passive grip, and biomimetic struc-ture. We created elastic silicone tarsal joints for several of these models and found that they produced linear stiffness within joint limits across different joint morphologies. Strain gauges positioned in CS locations on the trochanterofemur and tibia recorded strain while the leg stepped on a treadmill. Most, but not all, designs increased axial strain magnitude compared to previous data with no tarsus. Every tarsus design produced positive transversal strain in the tibia, indicating axial torsion in addition to bending. Sudden increases in tibial strain reflected leg slipping during stance. This data show how different aspects of the tarsus may mediate leg loading, allowing us to improve the mechanical biomimicry of future robotic test platforms.

Keywords: tarsus · campaniform sensilla · robot · Carausius morosus · passive compliance

Supported by NSF/DBI NeuroNex 2015317 to NSS, DFG Bu857/125-1 to AB, NSF CRCNS 2113028 to NSS and SNZ, and DFG DI 2907/1-1 (Project number 500615768, grant no. 233886668/GRK1960) to GFD.

The Author(s), under exclusive license to Springer Nature Switzerland AG 2023 F. Meder et al. (Eds.): Living Machines 2023, LNAI 14157, pp. 442–457, 2023. https://doi.org/10.1007/978-3-031-38857-6_32

Department of Mechanical and Aerospace Engineering, West Virginia University, Morgantown, WV, USA cg00022@mix.wvu.edu

² Institute of Zoology, University of Cologne, Köln, NRW, Germany

³ Department of Biomedical Sciences, Marshall University, Huntington, WV, USA

1 Introduction

Sensory feedback is an important part of how the nervous system produces robust and agile walking. Dynamic feedback from sense organs throughout an animal's body helps continually influence activity in the low-level motor networks and high-level control centers, which in turn adjust limb movements [4,37]. Furthermore, the sensory feedback available to the nervous system is highly dependent on an animal's mechanical structure [9,28]. An example of the interplay between sensing and mechanics in insects is found in the campaniform sensilla (CS), mechanoreceptors in various locations across the insect exoskeleton that detect strains in the cuticle as a proxy for force [13,26]. Due to their sensitivity to strain, leg CS are highly impacted by the loading state of the limb, its geometry, and its material properties. The effect of loading state has been shown in recordings from CS groups found on the trochanter, femur, and tibia in a variety of insects [37]. In particular, these CS robustly capture the rapid force changes during lift off and touch down, as well as a measure of the tonic loading throughout stance [30,38,40,41].

Biomimetic robots have great potential to help scientists investigate how mechanics influence sensors like the CS by providing a simplified platform on which to conduct neurobiological experiments [5,31]. Several of the authors of this work have recently investigated CS discharge during locomotion by implementing biomimetic strain sensing on robotic insect limbs [17,18,42]. As part of these investigations, a robotic leg modeled after a stick insect, *Carausius morosus*, was developed with biomimetic strain sensing in reported CS locations on the leg segments [42]. The robotic model showed the effects of morphological and environmental factors such as increased body weight or end effector slippage on leg strain and phenomenologically-modeled CS discharge.

Although many insects have complex tarsal anatomy, the previously developed robotic leg modeled the tarsus as a single semi-spherical, rigid segment at the distal end of the tibia [42]. The insect tarsus is typically comprised of several nested segments connected via elastic membranes [1,2]. These tarsal segments are actuated by a singular tendon, the retractor unguis tendon, originating in the femur and tibia, running through the underside of the tarsus, and connecting to a plate in the final segment, the pretarsus [29]. The pretarsus contains the tarsal claws, and in many types of insects an adhesive pad called the arolium [2,16]. In insects such as stick insects, the other tarsal segments additionally include anisotropic frictional pads called pulvulli or euplantulae [7,11,39]. This complex morphology is difficult to recreate for a robot, meaning the tarsus is often excluded from biomimetic insect robots [24]. However, the tarsus has a strong capacity to influence CS firing by mediating ground-leg interactions and subsequently affecting how loads from the substrate distribute throughout the leg. A list of mechanisms in the tarsus that potentially affect loading and the morphological aspects that cause them include: (1) Compliance to the terrain due to elastic joint membranes (2) Increased moment arm between the most proximal point of ground contact and the long axis of the tibia due to angling of the

tarsus; (3) Passive grip on ground surfaces from friction (euplantulae/pulvulli) and adhesive (arolium) pads; and (4) active grip with actuation of the claws.

To improve the biomimicry of our robotic animal models, and thus the accuracy of their predictions, it would be beneficial to understand the specific effects that these different tarsal mechanisms have on leg loading and the resulting CS firing. We could then design robotic tarsal segments that produce similar effects without the full biological complexity. However, it has not been inves-tigated how individual aspects of tarsal morphology influence loading sensing in the leg during walking. Several biological experiments have investigated the influence of different tarsal mechanisms on overall walking capability, such as the material properties of the frictional and adhesive pads [3,7], how the adhesive pads and claws work together to grip a variety of substrates [6,8], how joint elasticity affects passive retraction of the claws [16], and how the unguitractor mechanism allows 'latching' of the claws to a certain position [19]. Biorobotic studies have also begun to move in this direction by developing insect-inspired tarsi with passive compliance [17] to decrease walking impacts or exploring how tarsi with variable rigidity enable walking on complex substrates such as mesh [35]. However, none of these studies have addressed the impact on load sensing in their investigations. Additionally, experimental studies of CS responses in the legs are rarely conducted in walking animals [25,27,36], and sometimes include ablation of all or a portion of the tarsus [38,40]. These methods make it difficult to determine experimentally the effect of tarsal function and morphology on leg strain during walking.

To quantify how different aspects of tarsal morphology affect leg strain during stepping in our robots, we have developed a series of tarsal segments for our robotic C. morosus leg with varying degrees of compliance, passive grip, and biomimetic structure. To mimic the elasticity of the joint membranes and cuticle, we designed compliant tarsal joints with a combination of 3D printed plastic and silicone. Although the relative sizes of the tarsus and tibia differ in flies and stick insects [25,40], we used nano-CT scans of the tarsal segments of adult Drosophila melanogaster, another model organism for studying walking, to inform the shape of the tarsomere segments. We characterized the linearity and magnitude of the stiffness in our tarsal joints across different deflection directions, batches of silicone, and tarsal segment morphologies, and found they were linear within joint limits. Readings of the femoral and tibial strain in the axial and transverse directions were recorded for an average step on a treadmill for each of the developed tarsi designs. We found that including a tarsus typically increased strain magnitude by increasing the moment arm between the point of ground contact and the CS. The moment arm also increased the sensitivity of the strain to joint and leg plane angles. Occasions when the tarsus slipped on the substrate became more apparent in the tibial transverse strain signal due to sudden increases. Increasing passive grip seemed to have minimal impact on strain magnitude, but did prevent slipping. This work demonstrates the importance of modeling the tarsus in biomimetic robots.

2 Materials and Methods

2.1 Tarsal Segment Scans

Nano-CT imaging was performed for tarsal segments in the metathoracic legs of female wild-type *D. melanogaster* (Berlin- K, RRID:BDSC 8522) as described in reference [15]. Images were captured at the tarsal segment joints between segments 1 and 2, 3 and 4, and 5 and the pretarsus. Segmentations were initially rendered in Blender (Blender Foundation, Amsterdam, Netherlands), then decimated using MeshLab [10] for importing into CAD software. Images of the renderings for segments 1 and 2 and 5 and the pretarsus are shown in Fig. 1A. *D. melanogaster* was selected for imaging instead of *C. morosus* due to recent advancements in neuromechanical data collection making *Drosophila* a more universally studied insect for nervous system research [21,23,32]. Given the homology of tarsal morphology across insect species [34], we do not expect that modeling tarsomere joints after *D. melanogaster* will greatly impact our model of *C. morosus* stepping. Further, presently obtaining images from *D. melanogaster* allows for greater specificity in future *Drosophila* neurorobotic investigations.

2.2 Robotic Tarsus Construction

Three distinct 'styles' of robotic tarsi were designed with different amounts of biological abstraction. Each tarsus was designed with an overall length scaled 15:1 to the insect tarsus. Two of the styles were manufactured with or without silicone grip at the contact surfaces, resulting in five total designs. As labeled in Fig. 1B, each tarsus is designated 1–3 based on its style, with a * to denote the inclusion of exterior silicone in the design to increase passive grip between the treadmill and the tarsus.

A summary of each design style is as follows: Style 1, referring to Designs 1 and 1*, is a rigid cylindrical segment positioned at a 45° angle from the long axis of the tibia. This style is meant to isolate the effect of the moment arm created by the tarsus. Style 2 (i.e Designs 2 and 2*) retains this cylindrical shape and 45° offset, but additionally includes a compliant tibia-tarsus (TiTar) joint. This compliance is created via a ball-and-socket joint filled with silicone rubber to replicate the elastic properties of the tarsal membranes and cuticle (Fig. 1C). Style 3 adds full compliance through a biomimetic recreation of the six tarsal segments in the stick insect connected with these compliant silicone joints. Table 1 summarizes the morphological aspects of each design.

In order to create a high degree of biomimicry in our Style 3 segments, we designed ball-and-socket joints similar to our collected nano-CT images. We also maintained a similar contouring of the tarsal segments while ensuring manufacturing feasibility. Figure 1A shows a comparison of the joints between segments 1 and 2 and 5 and the pretarsus in the *Drosophila* nano-CT scans and our corresponding Style 3 designs. Each segment length was scaled proportionally from scanning electron microscopy (SEM) images of the stick insect tarsus [3,40]. Figure 1D shows a detailed look at Design 3 with the corresponding biological

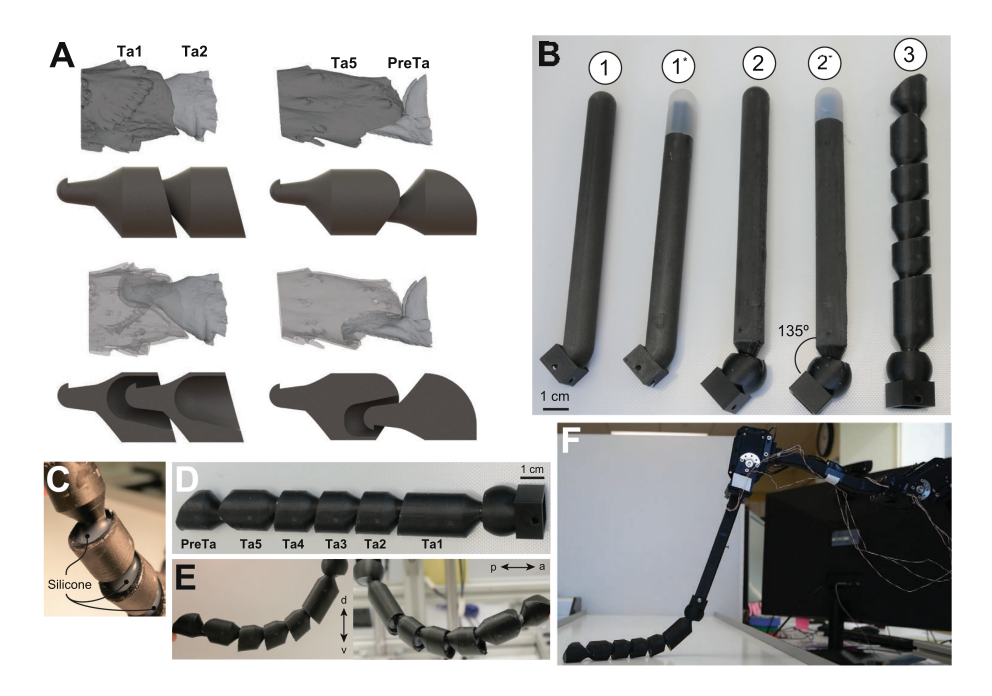


Fig. 1. Hardware designs for the robotic tarsal segments. (A) Comparisons of the nano-CT scans of *Drosophila* tarsal segments and the robotic segment designs for tarsal segments 1 and 2 (Ta1 and Ta2, respectively) and segment 5 (Ta5) and pretarsus. (B) The five tarsal morphologies labeled with their design designations. Three designs were tested with and without silicone grip components (silicone design denoted with a *). (C) Close-up view of the silicone interiors of the flexible segments, shown in Design 3. (D) Corresponding tarsal segments and notable biomimetic components labeled on Design 3. (E) Examples of the deflection capability of Design 3 in extension (left) and supination/pronation movements (right). (F) Leg setup with a Design 3 tarsus affixed.

Table 1. A summary of the morphological aspects of each tarsi design.

	Moment Arm	Compliance	Structure	Grip
Design 1	Yes	None	Simplified	No
Design 1*	Yes	None	Simplified	Yes
Design 2	Yes	TiTar	Simplified	No
Design 2*	Yes	TiTar	Simplified	Yes
Design 3	Yes	All Joints	Biomimetic	No

segments labeled. We omitted the claws and other aspects of active grip from our designs in this study due to the additional complexity of the tendon mechanism. Additionally, previous work in cockroaches suggests that removal of claws does

not affect walking behavior on smooth surfaces where friction/adhesive pads would be dominant in maintaining grip [22].

Each tarsus design was manufactured from a combination of 3D printed Onyx composite nylon (Markforged, Watertown, MA) and Dragon Skin 10 silicone rubber (Smooth-On Inc., Macungie, PA). To create the silicone joints, rigid joint surfaces were first coated with DOWSIL 1200 OS Primer (Dow, Midland, MI) to increase silicone adhesion, then placed in external fixturing replicating the equilibrium position of the joint. Silicone was poured into the joint and left to cure for a minimum of five hours. Silicone pads were manufactured in a similar manner with molds creating the contours of the pads; external tarsus surfaces were coated with primer to aid silicone adhesion, and mold surfaces were coated with Mann Ease Release 200 (Mann Release Technologies, Macungie, PA) to ensure easy extraction from the mold.

2.3 Compliant Joint Characterization

The silicone joints between segments in Styles 2 and 3 permit a large degree of deformation in multiple directions (Fig. 1E for Style 3). Each tarsal joint is capable of deflecting 15° in its most flexible directions before the rigid plastic of the joints touch, which we defined as the typical joint limits. Within these limits, the joint is assumed to behave like a typical ball-and-socket joint. To relate the moment applied to the joint (τ) to its angular deflection $(\Delta\vartheta)$ and evaluate the consistency of the manufacturing process, we collected force-deflection data with two different joint types: a tarsus-tarsus (TarTar) joint (i.e between two identical segments anywhere between segments 1 and 5 in Style 3; Fig. 2A) and a TiTar joint (found in Styles 2 and 3; Fig. 2B). For these tests, the proximal segment of each joint was affixed to the bottom plate of a Shimpo FGS-250W Manual Hand Wheel Operated Test Stand (Nidec-Shimpo America Corporation, Glendale Height, IL). A cable was routed through a hole in the distal segment and attached to the probe of a Shimpo FG-3008 Digital Force Gauge. The gauge was then vertically translated to apply force at intervals of 0.5 N. The angular deflection of the distal segment, $\Delta \vartheta$, and the angle of the cable from the vertical, ϑ_c , were both recorded through video capture. This process was repeated up to the limit of the joint. Figure 2C shows a picture of the test setup. Using these measurements along with the recorded force in the cable, T, the moment at each data point was calculated as $\tau = rT = rT\cos(\Delta\vartheta + \vartheta_c)$, where r is the moment arm length as shown in Fig. 2D. Each TarTar segment (n = 2) and TiTar segment (n = 1) was tested in dorsal and anterior-posterior deflection in at least two trials each. Ventral deflection was not tested due to the limited range of motion possible in the TarTar joint in this direction. The maximum force applied to the joint, and thus the number of data points per trial, varied depending on the deflection direction and joint morphology. For each trial, the stiffness coefficient k in Nm/rad was calculated as the slope of the curve fit to the τ vs. $\Delta \vartheta$ points with the y offset constrained to zero.

2.4 Stepping Experiments

Stepping experiments were conducted using a robotic leg modeled from the middle leg of a *C. morosus* stick insect walking on a treadmill (Fig. 1F). The leg setup is presented in full detail in ref. [42], but will be summarized briefly here. The leg is a 15:1 scale model of the insect's with the same segmental proportions. It includes actuated thorax-coxa (ThC), coxa-trochanter (CTr), and femur-tibia (FTi) joints. The ThC joint is mounted to a linear guide to allow free vertical movement, forcing the leg to support its weight as it steps. Two strain gauge rosettes are mounted on the leg to measure the transverse and axial strain data of each leg segment; one on the proximal dorsal face of the trochanterofemur (the trochanter and femur are fused in the stick insect), and one on the proximal dorsal face of the tibia. The locations and orientations of these rosettes are com-parable to that of major CS groups 3 and 4, 6A and 6B, respectively [14,30]. To control the leg, a MATLAB (MathWorks, Natick, MA) script commands servo-motor angles calculated from a desired footpath using inverse kinematics. The chosen footpath is modeled after that of *C. morosus* using a series of piecewise polynomials [12].

During a trial, a tarsal segment was affixed to the end of the tibia and the leg was commanded to step for six steps on the treadmill. Strain readings from each rosette were then recorded throughout stepping 60 Hz. The stride length of the footpath was adjusted to the scale of the robot leg, and the stepping period was set to 4s to dynamically scale leg movements (i.e ensure a similar balance of inertial, viscous, elastic, and gravitational forces as in the insect; for more information, please see ref. [42]). The joint trajectories of the leg were not altered throughout these trials. No additional body weight was considered during these tests, meaning the leg was only lifting its own weight (similar to the "baseline" tests in ref. [42].

The strain data from the first step was discarded due to irregularities in the start position. The remaining five steps' data were filtered by a moving median filter with a window of 13 timesteps. This filter removed single-timestep fluctuations due to noise without affecting the strain profile over time. The filtered strain data for each step was then averaged to produce a typical stepping strain profile.

3 Results

3.1 Compliant Joint Stiffness

To characterize the stiffness of our compliant silicone joints, we measured the moment required for angular displacements of each joint on TarTar and TiTar joint types within joint limits. We were primarily interested in identifying the degree of directionality in the stiffness, as well as the degree of stiffness variation between silicone castings and joint morphologies. To quantify these differences, we calculated and compared the stiffness coefficient, k, for each trial and the

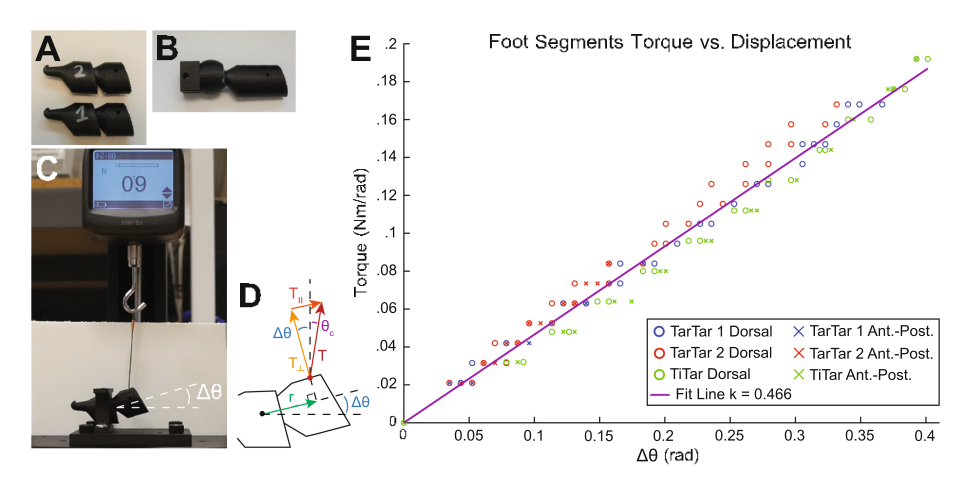


Fig. 2. Validation of the angular stiffness in our compliant silicone joints. (A) The two tarsus-tarsus (TarTar, i.e. between two identical segments anywhere between segments 1 and 5) joints tested. (B) The tibia-tarsus (TiTar) joint tested. (C) A frame from an extension trial with callouts showing the distal segment angular deflection, $\Delta\vartheta$ when force is applied. (D) A diagram of the force and angles present during deflection. (E) Torque vs. displacement graph for the TarTar (red for 1 and blue for 2) and TiTar (green) joints. Trials were conducted for extension (circle) and lateral movement (cross). The slope of the fit line (purple) to the entire dataset gives the stiffness coefficient of the joints. (Color figure online)

dataset as a whole. The results of all trials is presented as a torque vs. displacement graph in Fig. 2E. Each segment tested is represented by a different color; the first TarTar segment is blue, the second TarTar red, and the TiTar green. Dorsal deflection data points are represented by circles, and anterior-posterior deflection data points by crosses.

One immediately apparent feature of the data is the degree of linearity across trials. The average R-squared value of a line fit to a single trial's data was 0.994. Thus, the silicone-filled joints can be characterized as linearly elastic within typical joint limits. Furthermore, the segment stiffness does not appear to change drastically between different silicone pours, deflection directions, or joint morphologies. A line fit to the entirety of the dataset is shown in purple in Fig. 2E, with a slope of k = 0.466 Nm/rad. This line has an R-squared value of ≈ 0.98 , indicating a highly linear fit to the data. As such, for future projects with simi-lar tarsal segments we can assume a constant stiffness value of ≈ 0.46 Nm/rad across all segments for passive deflections within joint limits.

3.2 Strain Data

The primary purpose of this work is to explore how different aspects of tarsal morphology affect strain during walking. Thus, strain in the femur and tibia over an average step in the axial and transverse directions is presented in Fig. 3 for

each of the five tarsus designs we manufactured. In the strain plots, each style of tarsus is given a particular color; orange for Style 1, purple for Style 2, and green for Style 3. The designs without silicone grip have solid lines, and the designs with silicone grip have dashed lines. Data without a tarsus as in ref. [42] is also included in blue for reference. Positive strain represents compression, because CS are sensitive to compression [14]. The following sections describe these plots in more detail.

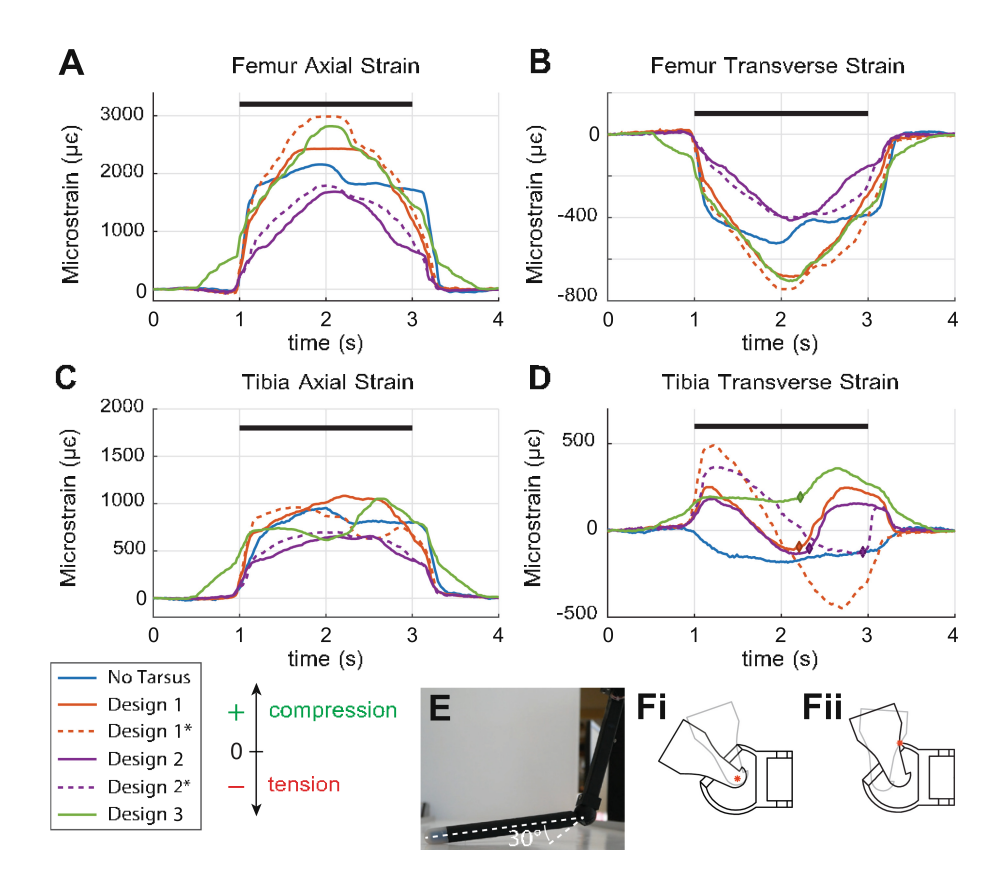


Fig. 3. Strain data for an average step for each tarsal design in the (A) femur axial, (B) femur transverse, (C) tibia axial, and (D) tibial transverse directions. Styles are given the same color, while the silicone grip designs are dashed and the non-silicone grip designs are solid. Data for no tarsus, as in ref [42], is included for reference (blue). The portion of the curve at which onsets of slip were observed are marked with dia-monds in (D). (E) Position of the Design 2* leg during stance. (F) Diagrams of the movement of tarsal segment 1 within the compliant TiTar joint during deflection (i) within joint limits and (ii) outside of joint limits. The pivot point of the joint during these movements is marked as a red *. (Color figure online)

Trochanterofemur Strain. For Styles 1 and 3, the overall magnitude of the trochanterofemoral strains exceeded that recorded with no tarsus by 25–50% in both directions. Style 2's peak strain, however, was $\approx 20\%$ less than that with no tarsus in both designs. The trochanterofemoral strains for different tarsus configurations also build and decay more gradually, resulting in a parabola-like curve typically peaking mid-stance.

Tibia Strain. Some effects from applying a tarsus occurred uniquely in the tibia strain data. Particularly in the transverse direction (Fig. 3D), strain readings became more sensitive to the pronation/supination of the leg. For Styles 1 and 2 this meant starting positive (compressive) in the first half of stance and becoming negative (tensile) as the tarsus became posterior to the FTi. This switch is most apparent in the Design 1* strain curve. Such strain propagation contrasts with the no-tarsus design, in which axial and transverse strains are scaled opposites, consistent with simple tension or compression of the leg surface (i.e. bending moments without axial torsion). However, every tarsus style broke this inversescale relationship, meaning that axial torsion was induced along the tibia. The Style 3 tarsus was the only design that created purely positive tibia transverse strain throughout the stepping cycle. Designs 1, 2, and 3 also exhibit a sudden increase in strain in the latter half of stance, approximately where they were observed to have slipped during testing (observed onsets of slip are marked with diamonds in Fig. 3D). Design 2* similarly produced a sharp increase in strain during the transition from stance to swing.

4 Discussion

In this study, we prototyped five tarsi for our robotic *C. morosus* leg to bet-ter understand which features of the tarsus, e.g., compliance, passive grip, and structure, most greatly impact the strain in the leg. As engineers, we seek the simplest design that will enable our robotic leg to accurately model the forces that the animal experiences during walking. To mimic the elasticity of insect joint membranes, we cast silicone hinges between tarsal segments. We characterized the stiffness and consistency of these joints. Finally, we recorded the strain experienced by the robotic leg as it stepped with each of the tarsi. The strain timecourses showed stark differences depending on the tarsus used. In subsequent sections, we propose explanations for the differences in leg strain among different Designs, comment on how the tarsus may aid in detecting leg slipping, and describe plans for future work.

4.1 Strain Magnitude

For Styles 1 and 3, the tarsus increased strain in the trochanterofemur and tibia segments relative to the no-tarsus baseline. This is likely because adding an angled segment increased the moment arm between the ground contact point and the FTi joint, increasing the strain of the tibia. However, Style 2's peak

strain was less than the no-tarsus baseline. This difference is likely due to the high degree of deflection in the compliant TiTar joint. As shown in Fig. 3E, the TiTar joint is deformed ≈30 deg from equilibrium, 15 deg over what we define as the joint limit. When this limit is reached, the highly compliant interior of the joint allows the joint axis to change from the center of the 'ball' of the distal segment (Fig. 3Fi) to the contact point between the distal segment and the proximal segment's outer walls (Fig. 3Fii), creating further joint deflection. It is presently unclear the precise angular stiffness of this additional deflection, or if the stiffness is linear as within the joint limits. However, such deflection does lessen the impacts felt during touch down by increasing the time for deceleration of the foot. We believe that these lesser impacts were subsequently not enough to overcome the static friction present in our current linear guide. Thus, some of the body weight was supported in the guide, lessening the forces distributed throughout the leg. We plan to address this issue in future studies by redesigning our guide system, as well as investigating the precise stiffness characteristics of our elastic joints outside of their normal limits.

4.2 Strain Profile

The strain in both locations on our leg builds and decays more gradually for our different tarsi. In the trochanterofemur, these changes created a parabola-like curve typically peaking mid-stance. Such a strain progression is due to the tarsal moment arm increasing sensitivity to pronation/supination of the leg. Consider the axial strain in Fig. 3A. The leg angles during stance in our joint trajectories (as shown in Fig. 3A in ref. [42]) result in the leg plane being nearly vertical halfway through stance. This position minimizes the magnitude of ground reaction force (GRF) components passively resisted by the joint structure and maximizing resulting moments induced by the GRF on the femur. Further supinating the leg throughout stance angles the leg plane, decreasing the force components transferred to the femur and naturally producing a parabola-like curve similar to that of the joint angles.

In the tibia, the leg plane sensitivity produced a switch in strain polarity across stance in Styles 1 and 2. This sign change aligns with the tarsus tip traveling caudally along the body during stance. The tip begins anterior to the FTi joint in the first half of stance, producing moments that place the dorsal tibia surface in compression (Fig. 3D). As stance progresses, the tarsus travels posterior to the FTi, generating moments that place the dorsal surface in tension. For Style 3, the strain remained compressive across stance. The high degree of elasticity in the joints could account for this difference, as the tarsus was able to twist and bend to great degrees throughout stance to maintain its initial con-tact point with the treadmill. This deformation could potentially create unique moment arms. Regardless of their specific morphology, each tarsus produced axial torsion along the tibia instead of simple bending moments, highlighting how additional tarsal moment arms can alter the types of bending produced in the leg during stepping.

4.3 Slipping Detection

Four of the five tarsal designs exhibited a sudden increase in transverse tibial strain during the latter half of stance phase: Designs 1, 2, 2*, and 3 (Fig. 3D). In designs without grip components, this rapid increase corresponded to observations of slipping between the foot and the treadmill (marked with diamonds in Fig. 3D). For Design 2*, the increase occurred during lift off of the foot at the onset of swing. This change may be due to a 'snap back' effect in which stored elastic energy from tarsus deflection attempts to accelerate the tarsus back to equilibrium upon slip. This restoring movement reconnects the foot with the treadmill, creating a secondary impact that produces tensile limb strain. Design 2* did not slip, but the high elastic moments produced during stance phase (described in Sect. 4.2) could similarly accelerate the tarsus back into the treadmill surface as the leg begins to quickly lift off the ground.

The effects of slip during pronation/supination presented here combined with previous data collected for lateral slipping [42] demonstrate how CS may contribute to the detection of slipping. In pronation/supination, the tibia seems integral to detecting slip, as the femur recordings were largely unaffected in either direction. Including a tarsus then makes slip more prominent in the tib-ial data by increasing the strain magnitude, changing strain directions through axial torsion, and producing a 'snap-back' effect through joint compliance. Both of these datasets align with biological recordings from stick insects showing the encoding of slip by the tibial CS [20]. It remains unclear how information from different CS locations is used in the nervous system, but indications of slipping in the tibial strains is one possible reason for collecting sensory information from this location.

4.4 Compliant Joint Robustness

The silicone membranes between the joints in three of our five designs satisfactorily mimicked the elasticity of insect joint membranes in a consistent man-ner between castings and joint morphologies. The connections were also robust enough to complete our tests without any detachment or tearing. However, characteristics such as the useful life of these joints, the maximum weight the joints can support, and the maximum deflection the joints can undergo without damage, are presently untested. Anecdotally, previous iterations of Style 2 in which the TiTar equilibrium position had the tarsus parallel to the tibia (i.e. similar to Design 3) were found to fail within a handful of steps after repeatedly deforming $\approx 90^{\circ}$, giving a rough upper limit to joint deflection. Such failure was characterized by the "ball" of the distal joint un-adhering from the silicone. Thus, exploring methods to improve the bond between the plastic and the silicone could improve joint performance. Such methods will be explored in future work, alongside characterizing the precise mechanical robustness of the current joints.

4.5 Conclusions and Future Work

This study reveals several concrete effects that a tarsus has on the strain magnitude and profile in various leg locations during stepping. Such data shows the potential importance of including a tarsus in our future biomimetic robot designs when investigating leg CS. However, it is presently difficult to say how biomimetic the recorded strain are, as no explicit strain data has been recorded in insects. CS discharge has certainly been recorded, but it is presently difficult to say the precise conversion between mechanical strain and firing rate, for exam-ple. Several authors of this work have previously developed a phenomenological model of CS discharge in response to leg strain and used it to hypothesize firing during stepping [33]. In future work, we plan to run our data through this model and compare the resulting discharge to biological data. This process will allow us to determine which aspects of our current work most reflect animal mechanics.

We also plan to address necessary simplifications made during this work to contain our scope and lay groundwork for future investigations. One simplification was the use of the tarsal morphology of flies, in which the tarsal segments are proportionally much longer than in stick insects, that may have amplified the effects of tarsal compliance during walking. Another such simplification was the exclusion of active grip due to the additional complexity of the unguitractor mechanism attached to the claws. Previous biological data has highlighted the limited role of the claws on smooth surfaces [22]. However, claws improve the general robustness of ground contact by maintaining grip on rougher surfaces [8]. Additionally, the extra grip force produced by the unguitractor mechanism would further improve ground contact, possibly reducing slipping. As the additional moment produced in the tarsus by the unguitractor is in the same direction as the joint elastic restoring moments, active grip may increase the magnitude of the 'snap-back' effect on the strain we observed upon slip. We plan to investi-gate how to include active grip into our model in future work by replicating the unguitractor mechanism.

Another simplification we made was to use the same stepping kinematics in our leg for each tarsal design to make their strain data directly comparable. This is markedly different from the nervous system, which is able to modulate stepping kinematics to account for changes in leg structure (e.g., missing segments). Given the high dependence of the Style 3 tarsi ground contact to the initial touchdown location of the pretarsus, the biomimetic tarsi design would likely benefit from adapted joint trajectories that account for tarsus length.

References

- 1. Arnold, J.: Adaptive features on the tarsi of cockroaches (Insecta: Dictyoptera). Int. J. Insect. Morphol. 3(3/4), 317–334 (1974). https://doi.org/10.1016/j.ymeth. 2019.07.013
- 2. Bässler, U.: Neural Basis of Elementary Behavior in Stick Insects. Springer, Berlin (1983). https://doi.org/10.1007/978-3-642-68813-3_6
- 3. Bennemann, M.: Biomimicry of the adhesive organs of stick insects (*Carausius morosus*). Ph.D. thesis, RWTH Aachen University (2015)

- Bidaye, S.S., Bockemühl, T., Büschges, A.: Six-legged walking in insects: how CPGs, peripheral feedback, and descending signals generate coordinated and adaptive motor rhythms. J. Neurophysiol. 119(2) (2018). https://doi.org/10.1152/jn. 00658.2017
- Buschmann, T., Ewald, A., von Twickel, A., Büschges, A.: Controlling legs for locomotion-insights from robotics and neurobiology. Bioinspir. Biomim. 10(4), 41001 (2015). https://doi.org/10.1088/1748-3190/10/4/041001
- Bußhardt, P., Gorb, S.N., Wolf, H.: Activity of the claw retractor muscle in stick insects in wall and ceiling situations. J. Exp. Biol. 214(10), 1676–1684 (2011). https://doi.org/10.1242/jeb.051953
- 7. Bußhardt, P., Wolf, H., Gorb, S.N.: Adhesive and frictional properties of tarsal attachment pads in two species of stick insects (Phasmatodea) with smooth and nubby euplantulae. Zoology 115(3), 135–141 (2012). https://doi.org/10.1016/j.zool.2011.11.002, http://dx.doi.org/10.1016/j.zool.2011.11.002
- 8. van Casteren, A., Codd, J.R.: Foot morphology and substrate adhesion in the Madagascan hissing cockroach, *Gromphadorhina portentosa*. J. Insect. Sci. 10(1), 1–12 (2010). https://doi.org/10.1673/031.010.4001
- Chiel, H.J., Beer, R.D.: The brain has a body: adaptive behavior emerges from interactions of nervous system, body and environment. Trends Neurosci. 20(12), 553–557 (1997). https://doi.org/10.1016/S0166-2236(97)01149-1
- Cignoni, P., Callieri, M., Corsini, M., Dellepiane, M., Ganovelli, F., Ranzuglia, G.: MeshLab: an open-source mesh processing tool. In: Scarano, V., Chiara, R.D., Erra, U. (eds.) Eurographics Italian Chapter Conference. The Eurographics Association (2008). https://doi.org/10.2312/LocalChapterEvents/ItalChap/ItalianChapConf2008/129-136
- Clemente, C.J., Dirks, J.H., Barbero, D.R., Steiner, U., Federle, W.: Friction ridges in cockroach climbing pads: Anisotropy of shear stress measured on transparent, microstructured substrates. J. Comp. Physiol. A 195(9), 805–814 (2009). https:// doi.org/10.1007/s00359-009-0457-0
- 12. Cruse, H., Bartling, C.: Movement of joint angles in the legs of a walking insect, *Carausius morosus*. J. Insect Physiol. 41(9), 761–771 (1995). https://doi.org/10.1016/0022-1910(95)00032-P
- Delcomyn, F.: Activity and directional sensitivity of leg campaniform sensilla in a stick insect. J. Comp. Physiol. A 168(1), 113–119 (1991). https://doi.org/10.1007/ BF00217109
- 14. Delcomyn, F., Nelson, M.E., Cocatre-Zilgien, J.H.: Sense organs of insect legs and the selection of sensors for agile walking robots. Int. J. Robot. Res. 15(2), 113–127 (1996). https://doi.org/10.1177/027836499601500201
- Dinges, G.F., Bockemühl, T., Iacoviello, F., Shearing, P.R., Büschges, A., Blanke,
 A.: Ultra high-resolution biomechanics suggest that substructures within insect mechanosensors decisively affect their sensitivity. J. Roy. Soc. Interface 19(190), 20220102 (2022). https://doi.org/10.1098/rsif.2022.0102
- Frazier, S.F., et al.: Elasticity and movements of the cockroach tarsus in walking. J. Comp. Physiol. A 185(2), 157–172 (1999). https://doi.org/10.1007/s003590050374
- 17. Goldsmith, C.A., Szczecinski, N.S., Quinn, R.D.: Neurodynamic modeling of the fruit fly *Drosophila melanogaster*. Bioinspir. Biomim. 15(6) (2020). https://doi.org/10.1088/1748-3190/ab9e52
- Goldsmith, C., Quinn, R.D., Szczecinski, N.S.: Investigating the role of low level reinforcement reflex loops in insect locomotion. Bioinspir. Biomim. 16, 065008 (2021). https://doi.org/10.1088/1748-3190/ac28ea

- Gorb, S.N.: Design of insect unguitractor apparatus. J. Morphol. 230(2), 219–230 (1996). https://doi.org/10.1002/(SICI)1097-4687(199611)230:2219::AID-JMOR83.0.CO;2-B
- 20. Harris, C.M., Szczecinski, N.S., Büschges, A., Zill, S.N.: Sensory signals of unloading in insects are tuned to distinguish leg slipping from load variations in gait: experimental and modeling studies. J. Neurophysiol. 128(5), 790–807 (2022). https://doi.org/10.1152/jn.00285.2022
- 21. Kohsaka, H., Nose, A.: Optogenetics in *Drosophila*. Adv. Exp. Med. Biol. 1293, 309–320 (2021). https://doi.org/10.1016/j.ymeth.2019.07.013
- 22. Larsen, G.S., Frazier, S.F., Zill, S.N.: The tarso-pretarsal chordotonal organ as an element in cockroach walking. J. Comp. Physiol. A 180(6), 683–700 (1997). https://doi.org/10.1007/s003590050083
- 23. Liessem, S., et al.: Behavioral state-dependent modulation of insulin-producing cells in *Drosophila*. Curr. Biol. 33(3), 449-463.e5 (2023). https://doi.org/10.1016/j.cub.2022.12.005
- 24. Manoonpong, P., et al.: Insect-inspired robots: bridging biological and artificial systems. Sensors 21(22), 1–44 (2021). https://doi.org/10.3390/s21227609
- 25. Merritt, D.J., Murphey, R.K.: Projections of leg proprioceptors within the CNS of the fly phormia in relation to the generalized insect ganglion. J. Comp. Neurol. 322(1), 16–34 (1992). https://doi.org/10.1002/cne.903220103
- Moran, D.T., Chapman, K.M., Ellis, R.A.: The fine structure of cockroach campaniform sensilla. J. Cell Biol. 48(1), 155–173 (1971). https://doi.org/10.1083/jcb. 48.1.155
- Noah, A.J., Quimby, L., Frazier, F.S., Zill, S.N.: Force detection in cockroach walking reconsidered: discharges of proximal tibial campaniform sensilla when body load is altered. J. Comp. Physiol. Sens. Neural Behav. Physiol. 187(10), 769–784 (2001). https://doi.org/10.1007/s00359-001-0247-9
- 28. Pfeifer, R., Iida, F., Gómez, G.: Morphological computation for adaptive behavior and cognition. Int. Congr. Ser. 1291, 22–29 (2006). https://doi.org/10.1016/j.ics. 2005.12.080
- 29. Radnikow, G., Bässler, U.: Function of a muscle whose apodeme travels through a joint moved by other muscles: why the retractor unguis muscle in stick insects is tripartite and has no antagonist. J. Exp. Biol. 157(1), 87–99 (1991). https://doi.org/10.1242/jeb.157.1.87
- 30. Ridgel, A.L., Frazier, S.F., Zill, S.N.: Dynamic responses of tibial campaniform sensilla studied by substrate displacement in freely moving cockroaches. J. Comp. Physiol. A 187(5), 405–420 (2001). https://doi.org/10.1007/s003590100213
- 31. Ritzmann, R.E., Quinn, R.D., Watson, J.T., Zill, S.N.: Insect walking and biorobotics: a relationship with mutual benefits. Bioscience 50(1), 23–33 (2000). https://doi.org/10.1641/0006-3568(2000)050[0023:IWABAR]2.3.CO;2
- 32. Scheffer, L.K., et al.: A connectome and analysis of the adult *Drosophila* central brain. eLife 9, 1–74 (2020). https://doi.org/10.7554/ELIFE.57443
- 33. Szczecinski, N.S., Dallmann, C.J., Quinn, R.D., Zill, S.N.: A computational model of insect campaniform sensilla predicts encoding of forces during walking. Bioinspir. Biomim. 16(6) (2021). https://doi.org/10.1088/1748-3190/ac1ced
- 34. Tajiri, R., Misaki, K., Yonemura, S., Hayashi, S.: Joint morphology in the insect leg: evolutionary history inferred from Notch loss-of-function phenotypes in *Drosophila*. Development 138(21), 4621–4626 (2011). https://doi.org/10.1242/dev.067330
- 35. Tran-Ngoc, P.T., Lim, L.Z., Gan, J.H., Wang, H., Vo-Doan, T.T., Sato, H.: A robotic leg inspired from an insect leg. Bioinspir. Biomim. 17(5) (2022). https://doi.org/10.1088/1748-3190/ac78b5

- 36. Zill, S.N., Moran, D.T.: The exoskeleton and insect proprioception III. Activity of tibial campaniform sensilla during walking in the American cockroach, Periplaneta americana. J. Exp. Biol. 94, 57–75 (1981)
- 37. Zill, S., Schmitz, J., Büschges, A.: Load sensing and control of posture and locomotion. Arthropod. Struct. Dev. 33(3), 273–286 (2004). https://doi.org/10.1016/j.asd.2004.05.005
- 38. Zill, S.N., Büschges, A., Schmitz, J.: Encoding of force increases and decreases by tibial campaniform sensilla in the stick insect, *Carausius morosus*. J. Comp. Physiol. A 197(8), 851–867 (2011). https://doi.org/10.1007/s00359-011-0647-4
- 39. Zill, S.N., Chaudhry, S., Büschges, A., Schmitz, J.: Force feedback reinforces muscle synergies in insect legs. Arthropod. Struct. Dev. 44(6), 541–553 (2015). https://doi.org/10.1016/j.asd.2015.07.001
- 40. Zill, S.N., Chaudhry, S., Exter, A., Büschges, A., Schmitz, J.: Positive force feedback in development of substrate grip in the stick insect tarsus. Arthropod. Struct. Dev. 43(5), 441–455 (2014). https://doi.org/10.1016/j.asd.2014.06.002
- 41. Zill, S.N., Ridgel, A.L., DiCaprio, R.A., Frazier, S.: Load signalling by cockroach trochanteral campaniform sensilla. Brain Res. 822(1), 271–275 (1999). https://doi.org/10.1016/S0006-8993(99)01156-7
- 42. Zyhowski, W.P., Zill, S.N., Szczecinski, N.S.: Adaptive load feedback robustly signals force dynamics in robotic model of *Carausius morosus* stepping. Front. Neurorobot. 17(January) (2023). https://doi.org/10.3389/fnbot.2023.1125171